



수치해석적 다짐 작용 연구: 공극률과 퇴적층 두께 변화에 미치는 영향

김예슬 · 이창열 · 이은영[‡]
 전남대학교 지구환경과학부

요 약

퇴적층의 두께와 형성 기간을 분석하는 것은 퇴적분지의 발달사를 이해하기 위한 분지 해석과 모델링 연구에서 중요하다. 분지 발달 과정에서 퇴적층은 깊이가 증가함에 따라 다짐 작용에 의해 두께가 감소하고, 이 두께 변화는 깊이에 따른 공극률 변화 경향(다짐 작용 경향)을 통해 계산이 가능하다. 이 연구에서는 대표적인 퇴적암상인 사암, 셰일, 탄산염암의 깊이에 따른 공극률 변화 자료를 기반으로, 암상에 따른 다짐 작용 경향의 범위를 지수 함수를 이용하여 정량화하였다. 그리고 다짐 작용이 퇴적층의 공극률과 두께 변화에 미치는 영향을 수치해석적 방법을 이용해 평가하였다. 사암은 초기 공극률의 범위가 좁고 깊이 증가에 따른 공극률 감소 경향이 비교적 일정하여, 다짐 작용에 의한 층두께의 변화 범위가 작다. 셰일은 약 2,000 m 깊이까지 공극률이 빠르게 감소한 후, 급격히 낮아진 감소율을 보이며 이는 퇴적층의 두께 변화에도 반영된다. 탄산염암은 초기 공극률의 범위가 넓고, 깊이 증가에 따른 공극률 감소 양상의 차이가 커서, 결과적으로 다짐 작용에 의해 감소한 퇴적층 두께 차이의 범위도 크게 나타난다. 이 수치 해석적 다짐 작용 연구의 정량적 분석 결과에서 나타난 각 암상들의 다짐 작용에 따른 공극률과 층두께 감소의 특징들은 퇴적분지의 생성과 발달 과정을 이해하기 위해 필요한 퇴적층 두께 복원과 침강사 그리고 지열 작용 분석에 영향을 끼치며, 이는 다짐 작용 경향이 분지 모델링 연구에서 중요한 요소이며 적절한 적용이 필요함을 보여준다.

주요어: 수치해석, 다짐 작용 경향, 공극률, 층두께, 분지 모델링

Yeseul Kim, Changyeol Lee and Eun Young Lee, 2018, Numerical analysis of sedimentary compaction: Implications for porosity and layer thickness variation. Journal of the Geological Society of Korea. v. 54, no. 6, p. 631-640

ABSTRACT: To understand the formation and evolution of a sedimentary basin in basin analysis and modelling studies, it is important to analyze the thickness and age range of sedimentary layers infilling a basin. Because the compaction effect reduces the thickness of sedimentary layers during burial, basin modelling studies typically restore the reduced thickness using the relation of porosity and depth (compaction trend). Based on the compilation plots of published compaction trends of representative sedimentary rocks (sandstone, shale and carbonate), this study estimates the compaction trend ranges with exponential curves and equations. Numerical analysis of sedimentary compaction is performed to evaluate the variation of porosity and layer thickness with depth at key curves within the compaction trend ranges. In sandstone, initial porosity lies in a narrow range and decreases steadily with increasing depth, which results in relatively constant thickness variations. For shale, the porosity variation shows two phases which are fast reduction until ~2,000 m in depth and slow reduction at deeper burial, which corresponds to the thickness variation pattern of shale layers. Carbonate compaction is characterized by widely distributed porosity values, which results in highly varying layer thickness with depth. This numerical compaction analysis presents quantitatively the characteristics of porosity and layer thickness variation of each lithology, which influence on layer thickness reconstruction, subsidence and thermal effect analyses to understand the basin formation and evolution. This work demonstrates that the compaction trend is an important factor in basin modelling and underlines the need for appropriate application of porosity data to produce accurate analysis outcomes.

Key words: numerical analysis, compaction trend, porosity, layer thickness, basin modelling

(Yeseul Kim, Changyeol Lee and Eun Young Lee, Faculty of Earth System and Environmental Sciences, Chonnam National University, Gwangju 61186, Republic of Korea)

[‡] Corresponding author: +82-62-530-3450, E-mail: eun.y.lee@chonnam.ac.kr

1. Introduction

Compaction in sedimentary rocks is generally considered as the dimensional change of accumulated porous rock due to increasing burial depth. It is commonly assumed to be equivalent to the reduction of porosity (pore volume) by grain rearrangement and compression. Mechanical porosity reduction is generally caused by vertical effective stress corresponding to the weight of the overlying rock and water column. A variety of empirical and experimental equations have been developed to quantify the compaction based on porosity values, which typically show exponentially decreasing porosity with increasing depth or vertical effective stress (e.g., Athy, 1930; Mondol *et al.*, 2007). This relation has been studied for diverse sedimentary rocks (e.g., Sclater and Christie, 1980; Schmoker and Halley, 1982; Bond and Kominz, 1984; Kominz *et al.*, 2011; Nooraiepour *et al.*, 2017) due to their importance in basic and applied earth science studies. It is particularly crucial in quantifying basin subsidence as well as in evaluating the quality of hydrocarbon reservoirs and geologic storage sites.

To understand the formation and evolution of a sedimentary basin in basin analysis and modelling, it is necessary to investigate the stratigraphic framework (e.g., thickness, age range) of sedimentary layers forming a basin's internal structure. However, the observed sedimentary layer at present does not directly represent the sedimentation during a basin's formation time, because the initial thickness of the layer is compacted during burial. To apply this change to basin modelling, forward basin modelling successively reduces the initial thicknesses of sedimentary layers through time and depth (e.g., Kusznir *et al.*, 1995). Conversely, backward basin modelling restores the thicknesses of compacted sedimentary layers using the decompaction process (e.g., Escalona and Mann, 2011). To compact or restore the thickness of a sedi-

mentary layer, many basin modelling studies have used the relationship between porosity and depth, often referred to as 'compaction trend' (Lee *et al.*, 2019). Due to absence of appropriate onsite compaction trends, however, some basin modelling studies have applied well known or published parameters (e.g., Sclater and Christie, 1980) to reconstruct a sedimentary layer based on its primary lithology. It is not apparent whether regional compaction trends are applicable to other basins developed in different tectonic setting, depositional system or temperature history. Moreover, since a lithology-based compaction trend is often estimated from porosity data of a particular sedimentary layer in a basin, the trend cannot reflect the complete trend through the full basin profile. It is likely that a locally calibrated trend cannot represent the primary compaction trend of a sedimentary basin, which can affect the process to compact or restore sedimentary layers in the basin modelling (Giles, 1997).

To quantify the lithology-based compaction through the full basin profile, this study analyzes compaction trend ranges based on the extent of compaction trends compiled for representative sedimentary rocks infilling basins; sandstone, shale and carbonate. Using these quantified compaction trend ranges, numerical analysis of sedimentary compaction is conducted to evaluate porosity and layer thickness variation at specific trends within each range. This study aims to (a) quantitatively determine the compaction trend ranges of sandstone, shale and carbonate, (b) conduct numerical compaction analysis using the compaction trend ranges and (c) investigate the influence of compaction on porosity and layer thickness variations with depth. This numerical analysis enables us to exclude influenceable external factors (e.g., temperature, fluid flow) and to avoid limitations (e.g., depth, stress, time) which are present in previous compaction studies.

2. Materials and Methods

2.1 Quantification of compaction trend range

This study quantifies lithology-based compaction trends as an attainable range concept, based on compilation plots of field-based compaction trends of sandstone, shale and carbonate arranged by Giles (1997) (Fig. 1). The compaction trend range of each lithology is determined by three sets of exponential curves; low-end curve, mean curve and high-end curve. Using Microsoft Excel and MATLAB software, the best-fitting exponential curves are estimated from relations of porosity

(%) and depth (m) data corresponding to low-end, mean and high-end points in the compaction trend range, which are quantified in consideration of the determination coefficient (overall above 0.97). Each curve is arranged as;

$$\phi = \phi_0 \exp(-y/c) \quad (1)$$

where ϕ : porosity at depth y (m), ϕ_0 : initial porosity at surface, and c : compaction coefficient (Fig. 2a). The compaction coefficient (c) is determining the slope of the compaction curve, which means that the initial porosity declines to $1/e$ of its orig-

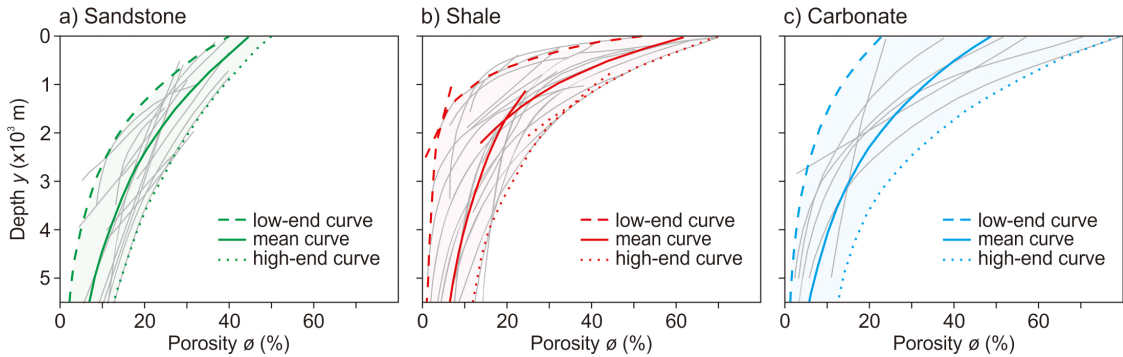


Fig. 1. Compilation plots of published compaction trends (gray lines) of a) sandstone, b) shale, c) carbonate (Giles, 1997). The compaction trend range of each lithology is defined by three sets of exponential curves; low-end curve (dashed line), mean curve (solid line) and high-end curve (dotted line).

Table 1. Exponential curves estimated from compaction trend ranges of sandstone, shale and carbonate. Low-end, mean and high-end curves of each lithology are presented exponentially in relationship of porosity (%) and depth (m) as $\phi = \phi_0 \exp(-y/c)$, where ϕ : porosity at depth y , ϕ_0 : initial porosity at surface, c : compaction coefficient.

| Lithology | Curve type | Exponential equation |
|-----------|------------|--|
| Sandstone | low-end | $\phi = 40 \exp(-y/1909)$ |
| | mean | $\phi = 44 \exp(-y/2966)$ |
| | high-end | $\phi = 49 \exp(-y/4040)$ |
| Shale | low-end | $\phi = 50 \exp(-y/764)$ (0 to 2,040 m) |
| | | $\phi = 6 \exp(-y/3560)$ (2,040~ m) |
| | mean | $\phi = 62 \exp(-y/1472)$ (0 to 1,680 m) |
| | | $\phi = 33 \exp(-y/3299)$ (1,680~ m) |
| | high-end | $\phi = 69 \exp(-y/2000)$ (0 to 1,420 m) |
| | | $\phi = 52 \exp(-y/3343)$ (1,420~ m) |
| Carbonate | low-end | $\phi = 23 \exp(-y/1846)$ |
| | mean | $\phi = 49 \exp(-y/2566)$ |
| | high-end | $\phi = 78 \exp(-y/2574)$ |

inal value at a depth of $1/c$ meters. Single exponential curves are used to represent the compaction trend range of sandstone and carbonate, while sets of two exponential curves are applied to define the compaction trend range of shale to fit better the underlying data.

The compaction trend ranges of sandstone, shale and carbonate with their low-end curve, mean curve and high-end curve are shown in Figure 1. This study provides estimated equations for each curve in Table 1. In the compaction trend range of sandstone, the initial porosities of low-end, mean and high-end curves are 40%, 44% and 49%, respectively, with compaction coefficients of 1909, 2966 and 4040. The compaction trend range of shale shows that the initial porosities of low-end, mean and high-end curves are 50%, 62% and 69%, respectively. To find better fitting trend, sets of two exponential curves are used to represent the compaction trend range of shale. Based on empirically defined inflection points, the intersecting depth of the two curves is estimated at 2,040 m in the low-end curve, 1,680 m in the mean curve and 1,420 m in the high-end curve. At these depths, the compaction coefficient changes from 764 to 3560 in the low-end curve, 1472 to 3299 in the mean curve and 2000 to 3343 in the high-end curve. In the compaction trend range of carbonate, the

initial porosities of low-end, mean and high-end curves are 23%, 49% and 78%, respectively, and the compaction coefficients of the curves are 1846, 2566 and 2574.

2.2 Numerical analysis of sedimentary compaction

This study conducts numerical analysis based on the isostatic balance of accumulated sedimentary layers and compacted sedimentary layers (Fig. 2b). Successive sedimentation is accomplished by stacking the new sedimentary layer on the surface of pre-accumulated layer. When the new layer piles up on the top of pre-accumulated layer, the total thickness of accumulated layers is reduced by the compaction effect with simultaneous release of pore water, which follows the exponential curve of porosity reduction with increasing burial depth in their compaction trend (Fig. 2a). This study assumes that the released water is stacked up on the surface of accumulated layers. The total thickness of compacted layers is calculated using the isostatic balance ($P_{B1}=P_{B2}$) between the basal pressure (P_{B1}) of the new layer (P_D) and pre-accumulated layer(s) (P_S) and the basal pressure (P_{B2}) of the compacted layers (P_C) and released water (P_W) (Fig. 2b);

$$P_{B1} = P_{B2} \quad (2)$$

$$P_D + P_S = P_W + P_C \quad (3)$$

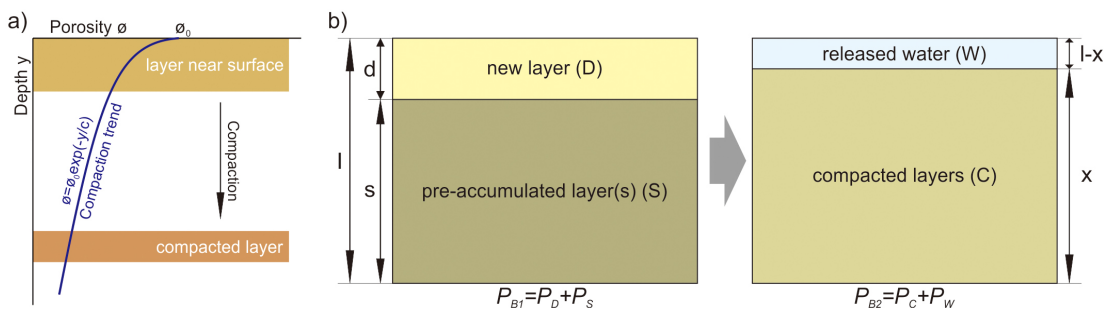


Fig. 2. a) Schematic diagram showing compaction process of a sedimentary layer with exponential compaction trend (porosity-depth relation) and equation (revised from Lee *et al.*, 2019). b) Concept of the isostatic balance ($P_{B1}=P_{B2}$) between the basal pressure (P_{B1}) of the new layer (P_D) and pre-accumulated layer(s) (P_S) and the basal pressure (P_{B2}) of the compacted layers (P_C) and released water (P_W). d , s , l and x : thicknesses of new layer, pre-accumulated layer(s), accumulated layers and compacted layers.

Table 2. General density values for sedimentary grains and water.

| Parameter | Density, kg·m ⁻³ |
|-----------|-----------------------------|
| Sandstone | 2650 |
| Shale | 2720 |
| Carbonate | 2710 |
| Water | 1000 |

The basal pressure of each layer (ρ_B) is defined as $P_B = \int_0^h \rho_b g dy$ using the thickness of each layer (h), bulk density (ρ_b) and gravity (g). The bulk density (ρ_b) of each layer is evaluated from a function for volumes of sediment grains and water-filled pores, and the volume is derived from porosity value with depth (Allen and Allen, 2013);

$$\rho_b = \rho_g(1 - \phi) + \rho_w\phi \quad (4)$$

where ρ_g : sediment grain density, ρ_w : water density and ϕ : porosity value at any depth. This study uses general values for density parameters (Table 2) and porosity values evaluated from compaction trend ranges. The basal pressure is calculated based on bulk density values of the new layer (ρ_D), pre-accumulated layers (ρ_s) and compacted layers (ρ_c), and the isostatic balance is arranged as;

$$g\rho_D d + g \int_0^s \rho_s ds = g\rho_w(1 - x) + g \int_0^x \rho_c dx \quad (5)$$

where d , s , l and x : thicknesses of new layer, pre-accumulated layer (s), accumulated layers and compacted layers, respectively. The thickness of a compacted layer is calculated by rearranging equation (5), which is given by;

$$f(x) = \rho_D d + (s + d - x)\rho_w + \int_0^s \rho_s ds + \int_0^x \rho_c dx \quad (6)$$

To calculate the thickness of each compacted layer, this study uses the bisection method which is one of the root-finding methods of nonlinear equations in numerical analysis. The method re-

peatedly bisects an equation interval and then selects a subinterval to search a root for further processing. The numerical compaction analysis is computed entirely in MATLAB[®] version 8.6 (R2015b). The numerical layer accumulation is performed by stacking a 100 m thick new layer on top of pre-accumulated layer for one hundred times. In the sequential accumulation of 100 layers, each layer is subsequently compacted following exponential curves determining the compaction trend ranges of sandstone, shale and carbonate.

3. Results

3.1 Porosity variation with depth

Numerical compaction analysis is applied to the accumulation of 100 layers following the exponential curves of each compaction trend range (Table 1). Figure 3 shows the porosity variation in the relationship between porosity values and depth. Porosities decrease overall with increasing depth and become nearly stationary at deep burial, while the reduction trend is different depending on lithology. In the porosity variation applying the compaction trend range of sandstone (Fig. 3a), the reduction trend is relatively consistent with ~6%/km on average and maintains a constant porosity width from surface (0 m) to near 6,700 m in depth. Porosity values evaluated by the compaction trend range of shale decrease rapidly within 2,000 m (Fig. 3b). Based on inflection points, porosity of 50% at surface falls to 3% at 2,040 m in the low-end curve, 62% to 20% at 1,680 m in the mean curve and 69% to 34% at 1,420 m in the high-end curve. Below these depths, the porosity reduction slows down significantly. Initial porosities of carbonate are distributed widely between 23% and 78%, which leads to the large variability of porosity reduction (Fig. 3c). The two end curves bounding the carbonate porosity range show significantly different results. Porosity of the low-end curve de-

increases from 23% to 0.3% at 8,112 m with a reduction rate of 3%/km on average, while porosity of the high-end curve shows fast decrease from 78% to 18.4% at 3,720 m with 16%/km on average.

3.2 Layer thickness variation with depth

Layers are stacked 100 times and compacted successively by numerical compaction analysis using the compaction trend ranges of sandstone, shale and carbonate (Table 1). The resulting plots of

layer thickness with depth are presented in Figure 4. Generally, the initial thickness (100 m) decreases rapidly between surface and ~2,000 m in depth, below which the thickness reduction slows down. The layer thicknesses of sandstone are distributed in a narrow range with depth, and the resulting curves show similar reduction trend and rate (Fig. 4a). This corresponds to similar thicknesses of the deepest layers which are 61 m in the low-end curve, 58 m in the mean curve and 56 m in the

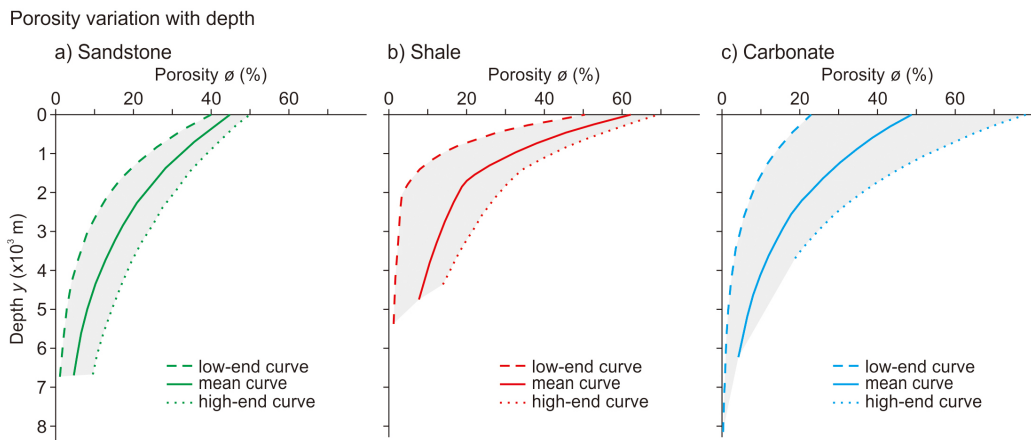


Fig. 3. Plots of porosity variation with depth; a) sandstone, b) shale, c) carbonate. Total 100 layers are accumulated and compacted following the exponential curves from the compaction trend range of each lithology. The porosity range with depth is presented using applied curves; low-end curve (dashed line), mean curve (solid line) and high-end curve (dotted line).

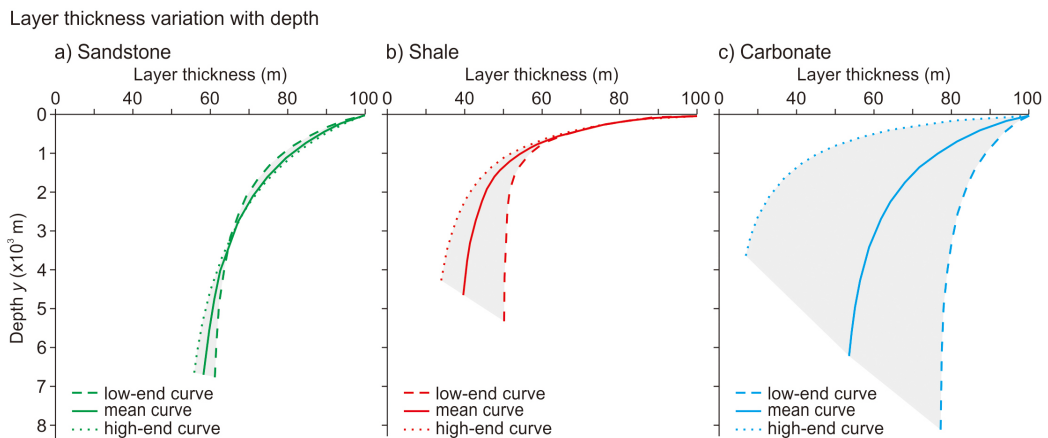


Fig. 4. Plots of layer thickness variation with depth; a) sandstone, b) shale, c) carbonate. Total 100 layers are accumulated and compacted following the exponential curves from the compaction trend range of each lithology. The layer thickness range with depth is presented using applied curves; low-end curve (dashed line), mean curve (solid line) and high-end curve (dotted line).

high-end curve. The final depth (total thickness) of the accumulated 100 layers is 6,738 m, 6,742 m and 6,674 m in the low-end, mean and high-end curves, respectively. The curves overlap where the layers reach around 3,500 m in depth and 64 m in layer thickness. In the layer thickness plot of shale (Fig. 4b), the thickness reduction trends of applied curves are almost identical and rapid in the shallow depths (~1,000 m) until the layers are compacted to around 60 m in thickness. After the rapid reduction, the rate decelerates abruptly, and the layer thickness of the low-end curve becomes constant with depth. The thickness of the deepest layer is 50 m in the low-end curve, 40 m in the mean curve and 34 m in the high-end curve. The final depth (total thickness) of the accumulated 100 layers is 5,387 m, 4,730 m and 4,348 m in the low-end, mean and high-end curves, respectively. In the carbonate-based compaction, thicknesses of compacted layers are widely distributed, which result in largely different reduction trends (Fig. 4c). The low-end curve shows slow reduction overall, while the high-end curve causes rapid reduction of layer thickness with depth, especially until around 1,500 m deep. The thickness of the deepest layer is 77 m in the low-end curve, 54 m in the mean curve and 27 m in high-end curve. The final depth (total thickness) of the accumulated 100 layers is 8,112 m, 6,264 m and 3,720 m in the low-end, mean and high-end curves, respectively.

Figure 5 presents the cumulative thickness range with layer accumulation. In a sedimentary basin, the total thickness of accumulated sedimentary layers corresponds to the depth of basement surface, and the chronologically arranged total thickness is based on subsidence analysis (Lee *et al.*, 2019). Therefore, the numerical setting of Figure 5 is comparable to estimating the basement subsidence of a basin infilling with single lithology sediment, which is developed over a duration of 100 Ma with 100 m/Ma in sedimentation rate. When the

compaction trend range of sandstone is applied, the resulting three curves of cumulative thickness show little difference (Fig. 5a). The curves of shale have similar trend until near 20 layers and 1,300 m thick, and then diverge (Fig. 5b). The cumulative thicknesses of carbonate show substantially different trends depending on the applied curve (Fig. 5c). Due to low reduction rate of layer thickness, the cumulative thickness of

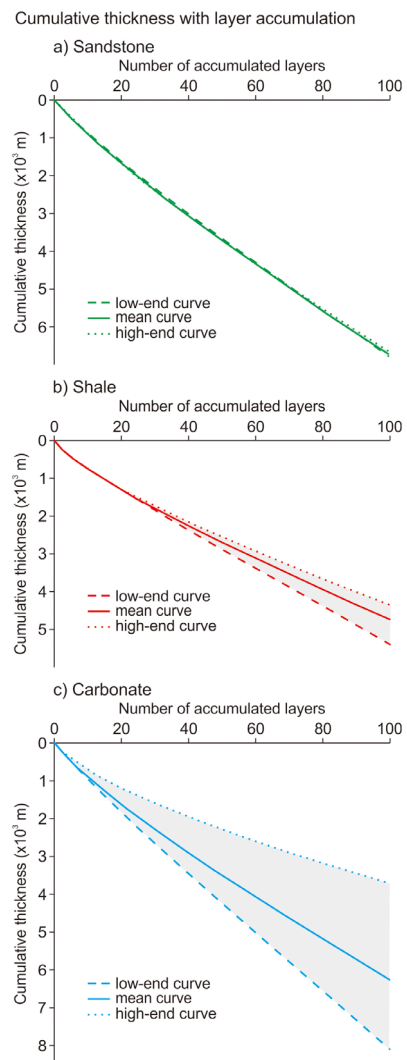


Fig. 5. Plots of cumulative thickness with layer accumulation; a) sandstone, b) shale, c) carbonate. The cumulative thickness range is presented using applied curves; low-end curve (dashed line), mean curve (solid line) and high-end curve (dotted line).

the low-end curve is significantly higher with relatively linear trending.

4. Discussion

The porosity loss during burial is affected mainly by three sets of interrelated processes; mechanical compaction, physicochemical compaction and cementation (Giles, 1997; Bogg, 2012; Allen and Allen, 2013). Mechanical compaction driven by loading of overlying sediments is mainly by grain sliding, mechanical rearrangement and grain crushing, which is dependent on burial depth and vertical effective stress. Physicochemical compaction is controlled by processes such as pressure solution, which is particularly important in carbonates due to their high chemical susceptibility. Cementation, which involves the filling of pore space by chemical precipitation, is related to temperature and fluid flow rather than to loading (Giles, 1997; Croizé *et al.*, 2010; Bjørlykke, 2014). From both experimental data and observations, siliciclastic sediments are compacted mechanically to about 2,000 m (e.g., Bjørlykke *et al.*, 1989; Stone and Siever, 1996), which corresponds to a fast variation of porosity and layer thickness in shallow depths presented in this study. Physicochemical compaction further reduces porosity and increases layer thinning during burial, and it is aided by cementation. In this study, the sandstone-based compaction presents thicknesses of compacted layers distributed in the narrow range. The steady compaction of sandstone is likely related to higher resistance of quartz grains to physicochemical compaction and associated cementation, and partly to well-sorted sandstone suffered less by mechanical compaction (e.g., Bjørlykke *et al.*, 1989; Bjørkum *et al.*, 1998; Ehrenberg and Nadeau, 2005; Bjørlykke, 2014). Compared to sandstone, shale and carbonate are more susceptible to physicochemical reaction and cementation which cause highly varying compaction effects. Because

of mud and clay in shale, including unstable minerals and other solids at greater depth (higher temperature), formation of kaolinitic clay minerals, partial dissolution of silicate grains, and precipitation of quartz and calcite cements take place commonly in the shale beds. In addition, the properties of mudstones are very strongly influenced by the biologically produced components like carbonates, silica and kerogen (Velde and Meunier, 2008; Thyberg and Jahren, 2011; Bogg, 2012; Bjørlykke, 2014). Despite of limited carbonate minerals (e.g., calcite, dolomite and aragonite), the porosity loss of carbonates is less predictable than siliciclastic rocks, at least in part due to diagenetic porosity modification and cementation (e.g., Giles, 1997; Ehrenberg and Nadeau, 2005; Croizé *et al.*, 2010). In carbonates, the porosity range results from highly variable grain shapes which often contain microscopic or macroscopic pores. Consequently, the porosity variations in carbonate are dominantly controlled by fabrics and textures (Anselmetti and Eberli, 1993). This characteristics cause that the wide range of porosities leads to high variability of layer thickness, which results in largely different final depths (total thicknesses) of accumulated layers.

In basin modelling, the compaction trend is used to reconstruct quantitatively the basin evolution through time and space. Forward basin modelling reduces successively the initial thicknesses of sedimentary layers, while backward basin modelling restores the thicknesses of compacted sedimentary layers. Since the total thickness of accumulated layers corresponds to the basement depth in a basin, the compaction trends and characteristics influence on subsidence analysis including total, tectonic, thermal subsidence, flexural and dip-slip backstripping (Lee *et al.*, 2019). In addition, due to the blanketing effect, the total thickness of sedimentary layers through time is applied to evaluate the amount of heat transfer from the underlying basement or crust to the sur-

face in the basin modelling (Wangen, 1995). This underlines that the basin evolution is affected by different compaction types based on the infill lithology or other effects, and the application of appropriate compaction trend is an important factor to reconstruct the evolution history of a sedimentary basin.

5. Conclusions

This study provides compaction trend ranges determined by exponential low-end, mean and high-end curves for sandstone, shale and carbonate. Each range is applied to numerical analysis of sedimentary compaction to investigate implications for porosity and layer thickness variation. The results present that each lithology has unique characteristics in compaction trend which are represented by different variation types and reduction rates of porosity and layer thickness with increasing depth. These are related to lithological features such as mineral composition, chemical reaction, sorting and grain shape. The compaction characteristics influence on sediment thickness reduction, subsidence and thermal effect during basin evolution. This study demonstrates that the appropriate application of compaction trend is an important factor for basin modelling to produce accurate evolution history of a sedimentary basin.

Acknowledgement

This work was supported by the National Research Foundation of Korea (2016R1D1A1B03930906 for Y. Kim) and the Korea Research Fellowship program funded by the Ministry of Science and ICT through the National Research Foundation of Korea (2017H1D3A1A01054745 for E.Y. Lee and C. Lee).

REFERENCES

Allen, P.A. and Allen, J.R., 2013, Basin analysis: Principles

- and application to petroleum play assessment. John Wiley & Sons, Chichester, 632 p.
- Anselmetti, F.S. and Eberli, G.P., 1993, Controls on sonic velocity in carbonates. *Pure and Applied geophysics*, 141, 2-4, 287-323.
- Athy, L.F., 1930, Density, porosity and compaction of sedimentary rocks. *AAPG Bulletin*, 14, 1, 1-24.
- Bjørkum, P.A., Oelkers, E.H., Nadeau, P.H., Walderhaug, O. and Murphy, W.M., 1998, Porosity Prediction in Quartzose Sandstones as a Function of Time, Temperature, Depth, Stylolite Frequency, and Hydrocarbon Saturation. *AAPG Bulletin*, 82, 4, 637-648.
- Bjørlykke, K., 2014, Relationships between depositional environments, burial history and rock properties. Some principal aspects of diagenetic process in sedimentary basins. *Sedimentary Geology*, 301, 1-14.
- Bjørlykke, K., Ramm, M. and Saigal, G.C., 1989, Sandstone diagenesis and porosity modification during basin evolution. *Geologische Rundschau*, 78, 1, 243-268.
- Bogg, S., 2012, *Principles of Sedimentology and Stratigraphy* (5th Edition). Pearson Prentice Hall, Upper Saddle River, N.J., 608 p.
- Bond, G.C. and Kominz, M.A., 1984, Construction of tectonic subsidence curves for the early Paleozoic miogeocline, southern Canadian Rocky Mountains: Implications for subsidence mechanisms, age of breakup, and crustal thinning. *Geological Society of America Bulletin*, 95, 2, 155-173.
- Croizé, D., Bjørlykke, K., Jahren, J. and Renard, F., 2010, Experimental mechanical and chemical compaction of carbonate sand. *Journal of Geophysical Research: Solid Earth*, 115, B11204, doi:10.1029/2010JB007697.
- Ehrenberg, S.N. and Nadeau, P.H., 2005, Sandstone vs. carbonate petroleum reservoirs: A global perspective on porosity-depth and porosity-permeability relationships. *AAPG Bulletin*, 89, 435-445.
- Escalona, A. and Mann, P., 2011, Tectonics, basin subsidence mechanisms, and paleogeography of the Caribbean-South American plate boundary zone. *Marine and Petroleum Geology*, 28, 8-39.
- Giles, M.R., 1997, *Diagenesis: A quantitative perspective - Implications for basin modelling and rock property prediction*. Kluwer Academic Publisher, Dordrecht, 526 p.
- Kominz, M.A., Patterson, K. and Odette, D., 2011, Lithology dependence of porosity in slope and deep marine sediments. *Journal of Sedimentary Research*, 81, 10, 730-742.
- Kuszniir, N.J., Roberts, A.M. and Morley, C.K., 1995, Forward and reverse modelling of rift basin formation. In: Lambiase, J.J. (eds.), *Hydrocarbon Habitat in Rift basins*. Geological Society, London, Special Publications,

- 80, 33-56.
- Lee, E.Y., Novotny, J. and Wagreeich, M., 2019, Subsidence Analysis and Visualization - For Sedimentary Basin Analysis and Modelling. Springer, Cham, 56 p.
- Mondol, N.H., Bjørlykke, K., Jahren, J. and Høeg, K., 2007, Experimental mechanical compaction of clay mineral aggregates-Changes in physical properties of mudstones during burial. *Marine and Petroleum Geology*, 24, 5, 289-311.
- Nooraiepour, M., Mondol, N.H., Hellevang, H. and Bjørlykke, K., 2017, Experimental mechanical compaction of reconstituted shale and mudstone aggregates: Investigation of petrophysical and acoustic properties of SW Barents Sea cap rock sequences. *Marine and Petroleum Geology*, 80, 265-292.
- Schmoker, J.W. and Halley, R.B., 1982, Carbonate porosity versus depth: a predictable relation for south Florida. *AAPG Bulletin*, 66, 12, 2561-2570.
- Sclater, J.G. and Christie, P.A., 1980, Continental stretching: An explanation of the post-mid-Cretaceous subsidence of the central North Sea basin. *Journal of Geophysical Research: Solid Earth*, 85, B7, 3711-3739.
- Stone, W.N. and Siever, R., 1996, Quantifying Compaction, Pressure Solution and Quartz Cementation in Moderately- and Deeply-Buried Quartzose Sandstones from the Greater Green River Basin, Wyoming. In: Crossey, L.J., Loucks, R., Totten, M.W. and Scholle, P.A. (eds.), *Siliciclastic Diagenesis and Fluid Flow: Concepts and Applications*. SEPM special publication 55, Society of Sedimentary Geology, 129-150.
- Thyberg, B.I. and Jahren, J., 2011, Quartz cementation in mudstones: Sheet-like quartz cement from clay mineral reactions during burial. *Petroleum Geoscience*, 17, 53-63.
- Velde, B. and Meunier, A., 2008, *The origin of clay minerals and weathered rocks*. Springer-Verlag, Berlin Heidelberg, 406 p.
- Wangen, M., 1995, The blanketing effect in sedimentary basins. *Basin Research*, 7, 4, 283-298.

Received : October 31, 2018

Revised : December 16, 2018

Accepted : December 17, 2018